Nanoparticle dispersion in porous media: Effects of attractive particle-media interactions

Deepak Mangal ⬤, Jacinta C. Conrad ⬤,[*] and Jeremy C. Palmer ⬤[†]

Department of Chemical and Biomolecular Engineering, University of Houston, Houston, Texas 77204, USA

We investigate the effects of physicochemical attractions on the transport of finite-sized particles in three-dimensional ordered nanopost arrays using Stokesian dynamics simulations. We find that weak particle-nanopost attractions negligibly affect diffusion due to the dominance of Brownian fluctuations. Strong attractions, however, significantly hinder particle diffusion due to localization of particles around the nanoposts. Conversely, under flow, attractions significantly enhance longitudinal dispersion at low to moderate Péclet number (Pe). At high Pe, by contrast, advection becomes dominant and attractions weakly enhance dispersion. Moreover, attractions frustrate directional locking at moderate flow rates, and shift the onset of this behavior to higher Pe.

I. INTRODUCTION

The dispersion of nano- to micron-sized particles through complex media underpins the efficacy of practical applications, including drug delivery [1,2], oil exploration and production [3], and separations processes such as gel electrophoresis [4] and chromatography [5]. The complex media in these settings may consist of solutions containing macromolecules, fluid mixtures, and solid porous materials. Thus, particle transport is controlled by multiple physical processes, including physicochemical and hydrodynamic interactions with the medium as well as coupling of the particle dynamics to local [6,7] and cooperative [8–10] medium relaxations. Understanding the contributions of these distinct processes to the dispersion of particles is essential to developing novel strategies for controlling their transport through complex media.

The transport of particles has been extensively studied using theory [11–13] and simulation [14–26]. Most computational studies of pore-scale transport, however, have focused on investigating the effects of medium geometry [11,27–29], packing arrangement [30,31], and flow conditions [31] on the dispersion of infinitesimal tracer particles. Particles whose size is comparable to length scales within the porous medium, such as throat or pore diameter, interact sterically as well as hydrodynamically with the medium during transport. Indeed, simulations of finite-sized particles in fibrous media under quiescent conditions have shown that their diffusivity markedly decreases with increasing solid volume fraction due to both steric hindrance and hydrodynamic drag [14,15,26,32,33]. These investigations have largely been carried out in the absence of nonsteric physicochemical interactions with the medium such as van der Waals and macromolecular depletion attractions and electrostatic forces, which are common in many practical settings. Notable exceptions include recent work showing that nonsteric interactions decrease the diffusivity of finite-sized particles in model gel networks [26,34].

Physicochemical attractions can lead to reversible and irreversible adsorption within porous media [35,36]. Most existing computational and theoretical studies that examine physicochemical attractions have also focused on the transport of infinitesimal tracer particles. Previous studies examining the effects of different variables, including sorbing conditions (equilibrium and kinetic) [37], retention factor [24,25], packing geometry [38], and particle shape [38,39], on particle transport under flow find, broadly, that adsorption strongly affects the dispersion of infinitesimal tracers. Comparatively few studies, by contrast, have addressed the complex multiphysics scenario encountered in many practical settings, where particle dispersion is affected by steric confinement and by attractions and hydrodynamic interactions (HI) with the medium. One recent study examined particle transport in geophysical fractures of varying aperture and attractive surface potential [40]. Particles were transported preferentially in regions of large aperture, and dispersion increased when the surface potential and local aperture were positively correlated. Nonetheless, fundamental open questions remain about how attraction strength and range influence particle dispersion across a broad range of flow conditions in different types of confining geometries.

In this study, we perform Stokesian dynamics (SD) simulations to investigate the effect of attractive interactions, in conjunction with steric and hydrodynamic forces, on particle transport. Specifically, we analyze the effect of attraction strength and range on particle diffusion and dispersion in three-dimensional square nanopost arrays. We find that weak attractions negligibly affect particle diffusion because dominant Brownian fluctuations allow particles to easily escape from the attractive wells around the nanoposts. Strong attractions, however, drive localization of the particles near the nanoposts and thereby hinder particle diffusion. For attractions of moderate strength, increasing the range further hinders diffusion. Conversely, under flow conditions, strong

---
[*]jcconrad@uh.edu
[†]jcpalmer@uh.edu

attractions significantly increase the longitudinal dispersion at low to moderate Péclet number (Pe) due to transient trapping of the particles near the nanoposts. At high Pe, where advection dominates, attractions weakly affect the dispersion. Increasing the attraction range at moderate strength enhances dispersion at low Pe, but has a negligible effect at higher flow rates. Finally, attractions frustrate directional locking, which reduces dispersion [41], at moderate flow rates and shift the onset of behavior to larger Pe.

II. METHODS

We performed SD simulations to investigate the effects of attractive interactions on particle transport through three-dimensional square arrays of nanoposts. Similar to previous studies [14,15,26,32–34], each nanopost was modeled as an immobile chain of tangential spherical beads of diameter d_{np} aligned along the z direction of the simulation cell (Fig. 1). The chains were arranged on periodic 3×3 square lattices in the x-y plane of the simulation cell [Fig. 1(a)]. The nanopost volume fraction in the system is given by $\phi = \pi d_{np}^2 / 6L^2$, where L is the spacing between adjacent posts. For convenience, the simulations were performed and analyzed using nondimensional units in which d_p, $k_B T$, and $\tau_d = 3\pi \eta d_p^3 / 4k_B T$ were chosen as characteristic length, energy, and time, respectively, where k_B is Boltzmann's constant, T is temperature, τ_d is the diffusive timescale, and η is the dynamic fluid viscosity.

The simulations were conducted under dilute conditions by considering the transport of a single particle through the nanopost arrays. Particle trajectories were propagated using the SD algorithm described in our previous study [33]. Hydrodynamic interactions were treated rigorously by including both short- and long-range components, using the Ewald summation method to accurately compute the latter [26,42–44]. Nonhydrodynamic interactions between the transported particle and beads in the nanopost were modeled using a Yukawa potential with a repulsive, hard-sphere core [26],

$$u(r_{ij}) = \begin{cases} -u_0 \exp{(-\kappa r_{ij})}, & r_{ij} \geqslant 0, \\ \infty, & r_{ij} < 0, \end{cases} \quad (1)$$

where u_0 is the magnitude of the potential strength, κ sets the range of the potential decay, and r_{ij} is the surface-to-surface distance between the particle and the nanopost bead (Fig. 2). We study values of u_0 and κ in the range 0–7 and 20–40, respectively, which are characteristic of the interactions (e.g., depletion) observed for particles in porous media [45,46]. A standard rejection scheme [26,32] was used to account for the hard steric repulsion for $r_{ij} < 0$. Flow was driven through the arrays by imposing a uniform suspension velocity $\mathbf{V}_\infty$ with orientation $\theta = \arccos{(\frac{\mathbf{V}_\infty \cdot \mathbf{a}}{|\mathbf{V}_\infty||\mathbf{a}|})}$ relative to lattice vector $\mathbf{a}$ [Fig. 1(a)]. The particle equations of motion were integrated using a time step dt in the range 10^{-7}–10^{-5}, depending on V_∞ and the strength of the attractive potential. Tests were performed in each case to confirm that the computed properties were insensitive to further reduction of dt ($<3\%$ variation). All other details of the SD simulations are identical to those reported in Ref. [33].

Transport properties were computed by averaging over 100 independent particle trajectories, using the standard error of
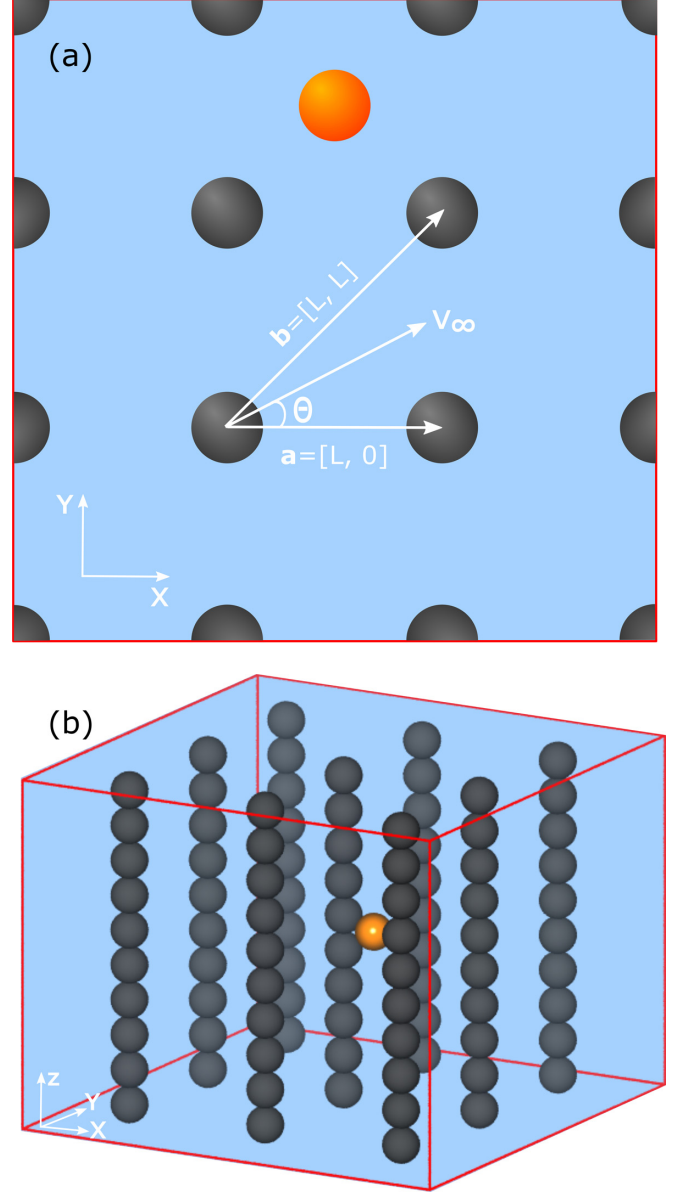

FIG. 1. (a) Two-dimensional orthographic projection of a square nanopost array in the x-y plane of the simulation cell. (b) Three-dimensional perspective view of a section of a square nanopost array. The spheres representing the nanoposts (gray, np) and the diffusing particle (orange, p) have the same diameter (i.e., $d_{np} = d_p$).

the mean to estimate statistical uncertainties. The particle diffusivity under quiescent conditions was obtained from the long-time limit of the ensemble-averaged, in-plane mean-square displacement (MSD), $D_q = \lim_{\Delta t \to \infty} \langle \Delta r^2(\Delta t) \rangle / 4\Delta t$. Similarly, the asymptotic longitudinal dispersion coefficient (dispersion in the direction of flow) D_L under flow conditions was calculated via [29,47]

$$D_L \equiv \lim_{t \to \infty} \frac{1}{2} \frac{d\sigma_L^2(t)}{dt}, \quad (2)$$

where $\sigma_L^2(t) = \langle (\Delta r_L(t) - \langle V_L \rangle t)^2 \rangle$ is the particle MSD evaluated in the frame of reference of the average longitudinal velocity $\langle V_L \rangle$. The velocity $\langle V_L \rangle$ was estimated from a linear fit
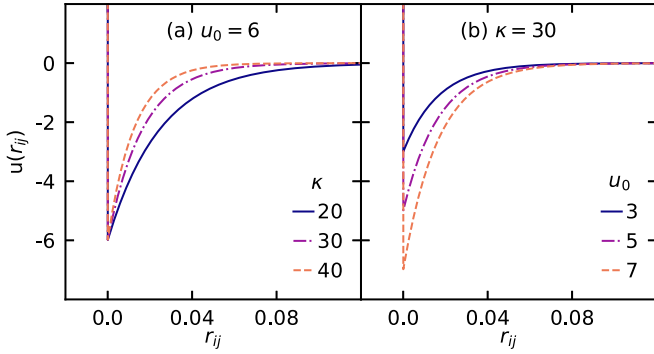
FIG. 2. Yukawa potential with repulsive core $u(r_{ij})$ [Eq. (1)] as a function of the surface-to-surface distance r_{ij} for (a) different u_0 and fixed $\kappa = 30$ and (b) different κ and fixed $u_0 = 6$.

to the average particle displacements over time. Both D_q and D_L were normalized by the diffusivity of the freely diffusive particle, $D_0 = k_B T / 3\pi \eta d_p$.

III. RESULTS AND DISCUSSION

We first examined the two-dimensional, in-plane particle diffusivity as a function of the potential strength u_0 for $\kappa = 30$ for different nanopost volume fractions ϕ. The normalized in-plane diffusivity D_q/D_0 is not strongly influenced by the presence of weak interactions (i.e., $u_0 \leqslant 3$) [Fig. 3(a)], indicating that thermal Brownian fluctuations allow the particles to easily escape the attractive wells around the nanoposts. Upon further increasing the potential strength, however, D_q/D_0 exhibits a gradual downturn, followed by a sharp decrease for $u_0 \geqslant 5$, suggesting that stronger attractions drive localization of the particles near the nanoposts. Increasing the range of the potential κ^{-1} also affects the particle diffusivity [Fig. 3(b)]. Whereas changing the potential range for $u_0 = 3$ has little effect on the diffusivity, D_q/D_0 steadily decreases with increasing κ^{-1} for $u_0 = 6$, suggesting that longer-range attractions increasingly hinder particle diffusion. Although D_q/D_0 decreases with increasing nanopost volume fraction ϕ due to the increase in confinement experienced by the particles, changing the potential strength and range results in similar trends across all values of ϕ examined. The sharp decrease of diffusivity at strong attraction strength is in qualitative agreement with a previous simulation study of transport in hydrogel matrices [26] and the behavior predicted by a theoretical model [48]. Moreover, in the absence of attractions ($u_0 = 0$), the three-dimensional diffusivity $D_{q,3D}/D_0$ is well described by a hydrodynamic model for hindered diffusion [49] [Fig. 3(c)]. As the potential strength is increased, progressively larger deviations from the prediction are observed because the model neglects the effects of attraction interactions.

Particle transport under flow conditions was investigated in a nanopost system with $\phi = 0.028$ by imposing a uniform suspension velocity $\mathbf{V}_\infty$ with a $\theta = 45°$ orientation with respect to the lattice vector $\mathbf{a}$ [Fig. 1(a)]. In the absence of attractions ($u_0 = 0$), the normalized average particle velocity $\langle V_L \rangle / V_\infty$ remains approximately constant and near unity as the flow magnitude $V_\infty = |\mathbf{V}_\infty|$ is varied, indicating that particles on
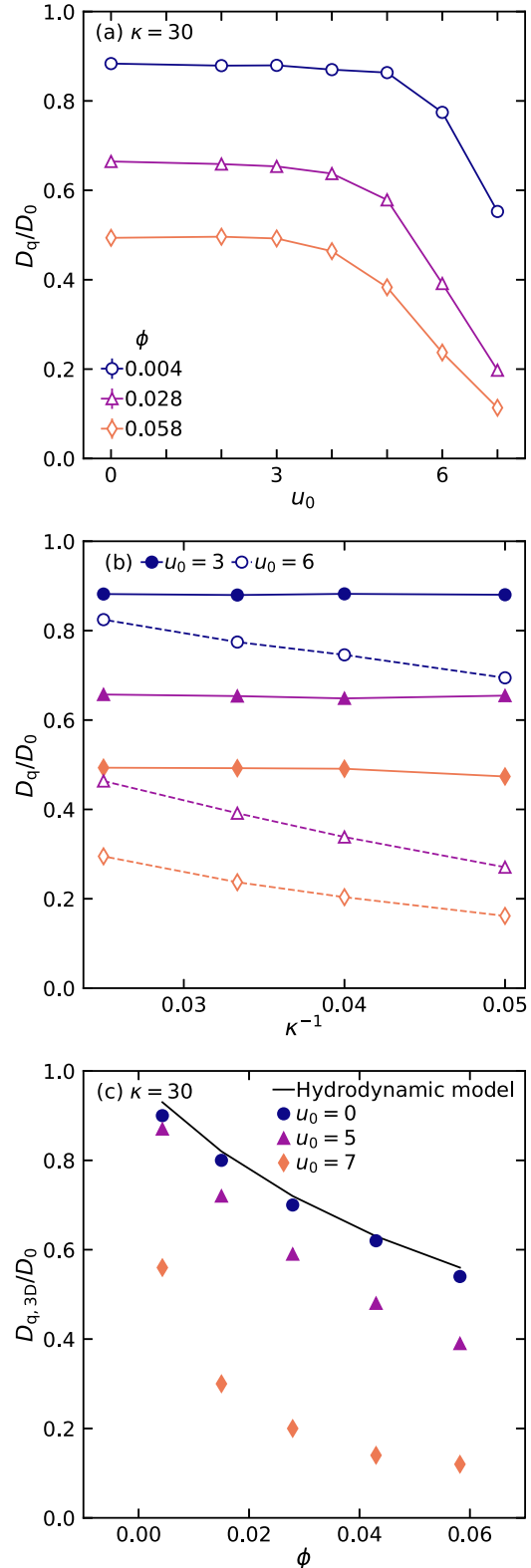

FIG. 3. Normalized in-plane diffusion coefficients D_q/D_0 as functions of (a) potential strength u_0 for $\kappa = 30$ and (b) potential range κ^{-1} for $u_0 = 3$ and 6. (c) Comparison of normalized three-dimensional diffusion coefficients $D_{q,3D}/D_0$ as functions of nanopost volume fraction ϕ with a hydrodynamic model for hindered diffusion [49]. Estimated uncertainties are smaller than the symbol sizes.
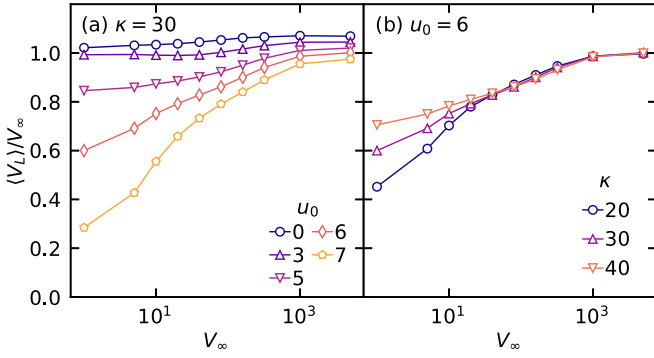
FIG. 4. Normalized average particle velocities $\langle V_L \rangle / V_\infty$ as functions of uniform suspension velocity V_∞ at flow orientation $\theta = 45°$ for (a) different u_0 and fixed $\kappa = 30$ and (b) different κ and fixed $u_0 = 6$. Estimated uncertainties are smaller than the symbol sizes.

average move at the same speed as the imposed flow (Fig. 4). For $u_0 \geqslant 5$, however, $\langle V_L \rangle / V_\infty$ is no longer independent of V_∞. For these attraction strengths, the normalized velocity is less than one for $V_\infty < 10^1$, and approaches unity as V_∞ is increased above 10^3. Further, the value of $\langle V_L \rangle / V_\infty$ decreases as u_0 is increased. Together, these trends reveal that sufficiently strong attractions with the nanoposts reduce the average velocity of the particles at low to moderate flow rates, consistent with localization or transient trapping of particles.

To further characterize the particle localization behavior, we computed the particle residence time t_R near the surfaces of the nanoposts as a function of suspension velocity V_∞ and attraction strength u_0 for a system with interaction range $\kappa = 30$. The residence time was defined as the duration spent within a thin shell around a nanopost, using a surface-to-surface distance cutoff of 0.1 to encompass the attractive well. Under quiescent conditions, the residence-time distribution $P(t_R)$ exhibits a sharp initial decrease at small t_R before crossing over to exponential decay at larger residence times [Fig. 5(a)]. The exponential tail of $P(t_R)$ becomes broader as the attraction strength u_0 increases. Similar behavior is observed under weak flow [$V_\infty = 5$; Fig. 5(b)]. As V_∞ increases at constant u_0, however, the exponential tail of the residence-time distribution narrows [Figs. 5(c) and 5(d)]. Additionally, $P(t_R)$ begins to exhibit a local minimum at small t_R. This local minimum arises from the competition between Brownian forces and advection near the cutoff boundary, where the effect of attractions is very small. For small $V_\infty \leqslant 5$, particles can easily move across the cutoff boundary by dominant Brownian motion, leading to a smooth and sharp decrease in $P(t_R)$ at small t_R. Upon increasing V_∞, however, the probability of the particles moving along the flow streamlines increases due to the greater effect of advection and enhances $P(t_R)$ for intermediate t_R, resulting in a local minimum at small t_R.

Previous studies showed that the characteristic residence time τ_R significantly affects solute dispersion [24,25]. Thus, we estimated the characteristic timescale τ_R associated with the exponential decay at large residence times by fitting the tail regions to $P(t_R) = ce^{-t_R/\tau_R}$, where c is a fitting constant [24,50]. The characteristic time τ_R increases in an approximately exponential fashion with increasing u_0 for all
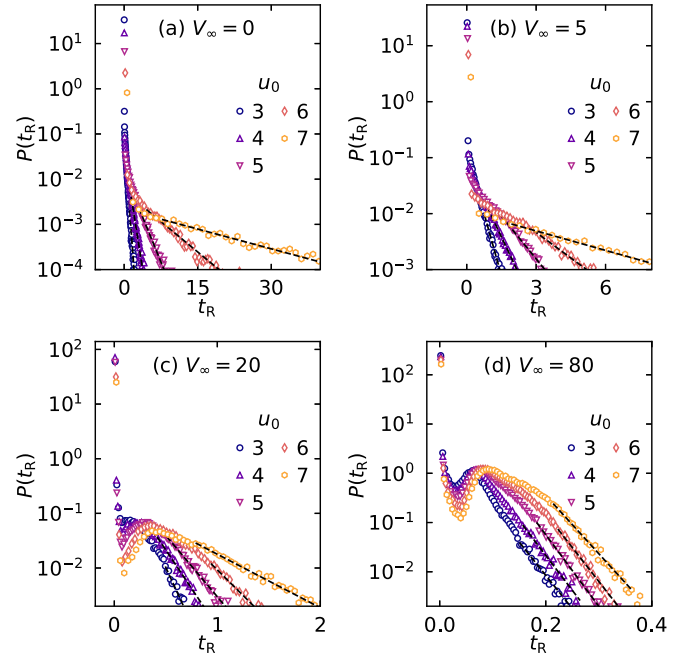

FIG. 5. Trap time distribution $P(t_R)$ for attractive potentials with different u_0 and fixed $\kappa = 30$. Distributions are shown for a uniform suspension velocity V_∞ of (a) 0, (b) 5, (c) 20, and (d) 80. The black dashed lines show fits to the function $P(t_R) = c \exp^{-t_R/\tau_R}$.

V_∞ examined (Fig. 6). This behavior is consistent with the strong decrease in the average particle velocity at a given V_∞ [Fig. 4(a)] and also with the Frenkel model for a first-order desorption process, which predicts that the average adsorption sojourn time will increase exponentially with the average adsorption energy [25,51,52]. Previous simulations examining the transport of short polymers on an attractive flat surface [53] and in crowded nanopost arrays [50] also reported an
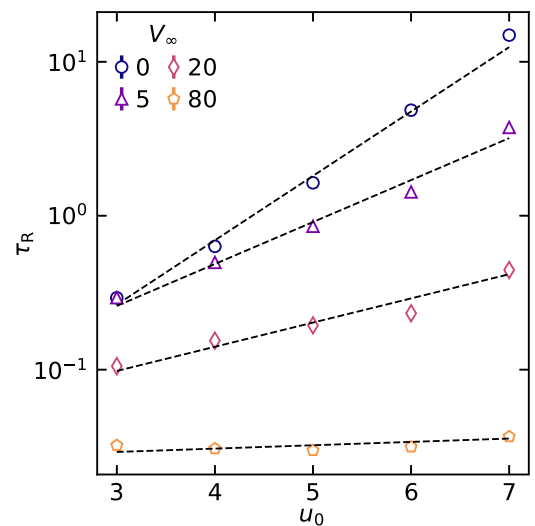

FIG. 6. Characteristic trapping time τ_R as a function of the magnitude of the potential strength u_0 for $\kappa = 30$ at different V_∞. The black dashed lines show fits to the function $\tau_R = c_1 \exp^{-c_2 u_0 / k_B T}$, where c_1 and c_2 are fitting constants.
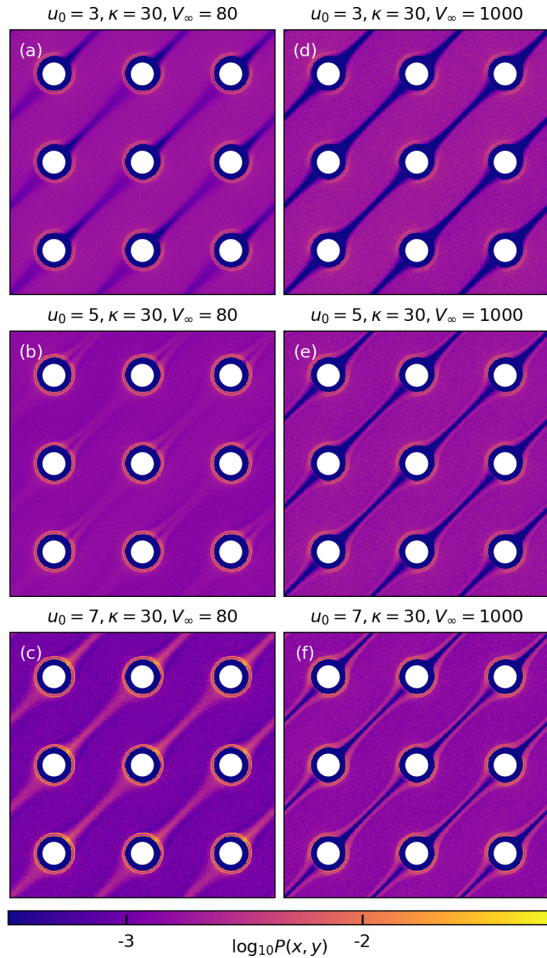
FIG. 7. Log-probability density distributions of particle positions $\log_{10} P(x, y)$ for u_0 of (a), (d) 3, (b), (e) 5, and (c), (f) 7 at V_∞ of (a)–(c) 80 and (d)–(f) 1000 for flow orientation $\theta = 45°$. The intense blue color corresponds to regions where $\log_{10} P(x, y) < -3$.

FIG. 8. Normalized longitudinal dispersion coefficients D_L/D_0 as functions of Pe at flow orientation $\theta = 45°$ for (a) different u_0 and fixed $\kappa = 30$ and (b) different κ and fixed $u_0 = 6$. Estimated uncertainties are smaller than the symbol sizes.

exponential decay in $P(t_R)$ and an increase in τ_R with increasing potential strength.

Next, to visualize the effect of u_0 on particle localization, we computed the log-probability density distribution of the particle positions in the x-y plane $\log_{10} P(x, y)$ for selected values of u_0 and V_∞ (Fig. 7). For low suspension velocity ($V_\infty = 80$), increasing u_0 alters the extent to which particles localize in the wake of the nanoposts. When $u_0 = 3$, the particles near the surfaces of the nanoposts are easily driven away by advection [Fig. 7(a)]. Upon increasing u_0, however, the particles cannot easily escape the attractive wells of the nanoposts due to the strong interactions. Strong attractions force particles to move along the surface of the nanoposts to the wake. Subsequently, particles are driven away from the nanoposts along the slow flow streamlines, which are oriented parallel to V_∞ [Figs. 7(b) and 7(c)]. By contrast, for $V_\infty = 1000$, hydrodynamic drag forces are dominant and increasing the attraction strength u_0 does not markedly alter the particle distribution [Figs. 7(d)–7(f)].

The changes in the residence times and particle distributions arising from variation in attraction strength and range are expected to affect dispersion. Hence, we examined the
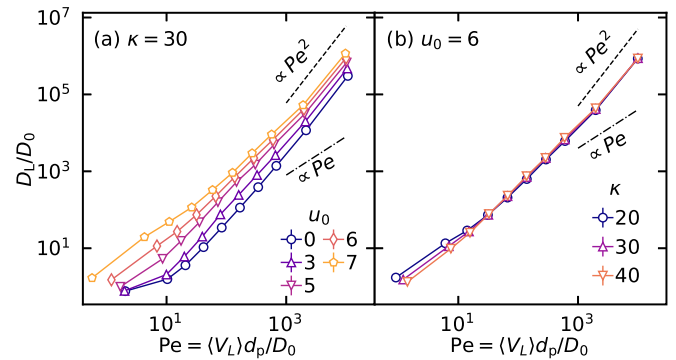
behavior of the normalized longitudinal dispersion coefficient D_L/D_0 as a function of the dimensionless Péclet number $Pe = \langle V_L \rangle d_p/D_0$ for various u_0 and κ. In the absence of attractions ($u_0 = 0$), D_L/D_0 initially increases gradually with Pe and then transitions to Pe^n scaling with $n \approx 2$ (i.e., Taylor-Aris dispersion behavior) for $Pe \gtrsim 10^2$ [Fig. 8(a)]. Upon increasing u_0 over the range 0–7, D_L/D_0 increases up to two orders of magnitude at low and moderate Pe (Pe $< 10^3$). In the presence of strong attractions ($u_0 > 3$), particles become more localized in the wake of the nanoposts, thereby leading to broader distribution along the flow direction. At very large Pe (Pe $> 10^3$), the effects of advection become dominant and D_L/D_0 only increases weakly with u_0, exhibiting a transition to quadratic scaling. By contrast, increasing the range of the potential κ^{-1} for fixed u_0 negligibly affects D_L/D_0, except for a slight increase at low Pe [Fig. 8(b)].

Finally, we investigated the effects of attractions on directional locking, which enables size-based separation of particles in deterministic lateral displacement (DLD) devices [22,54]. Sorting of suspended particles driven through periodic potential fields by directional locking has also attracted interest [12,13,16,17,19,20,23]. In our previous study of the influence of flow orientation on transport in square and hexagonal arrays with purely repulsive, nonhydrodynamic particle-nanopost interactions [41], we observed an abrupt decrease in average particle velocity and longitudinal dispersion for certain flow orientations slightly perturbed from primitive lattice vectors. This decrease was attributed to directional locking behavior in which steric interactions with the nanopost cause the particle dynamics to become dominated by advection along a specific vector over a finite range of θ [22].

In both the square and hexagonal arrays with $\phi = 0.058$, directional locking was most pronounced for flow orientations slightly perturbed from the lattice vector **a** (i.e., θ near 0°) [41]. Consequently, we investigated the effects of attraction in a square array with $\phi = 0.058$ for $\theta = 1.25°$. In the absence of attractive interactions (i.e., $u_0 = 0$), the in-plane log-probability density distribution $\log_{10} P(x, y)$ reveals strong direction locking along the lattice vector **a** at all V_∞ [Figs. 9(a)–9(c)]. With increasing V_∞, the distribution becomes increasingly narrow, reflecting enhanced directional locking. For $u_0 = 7$, however, the attractive interaction

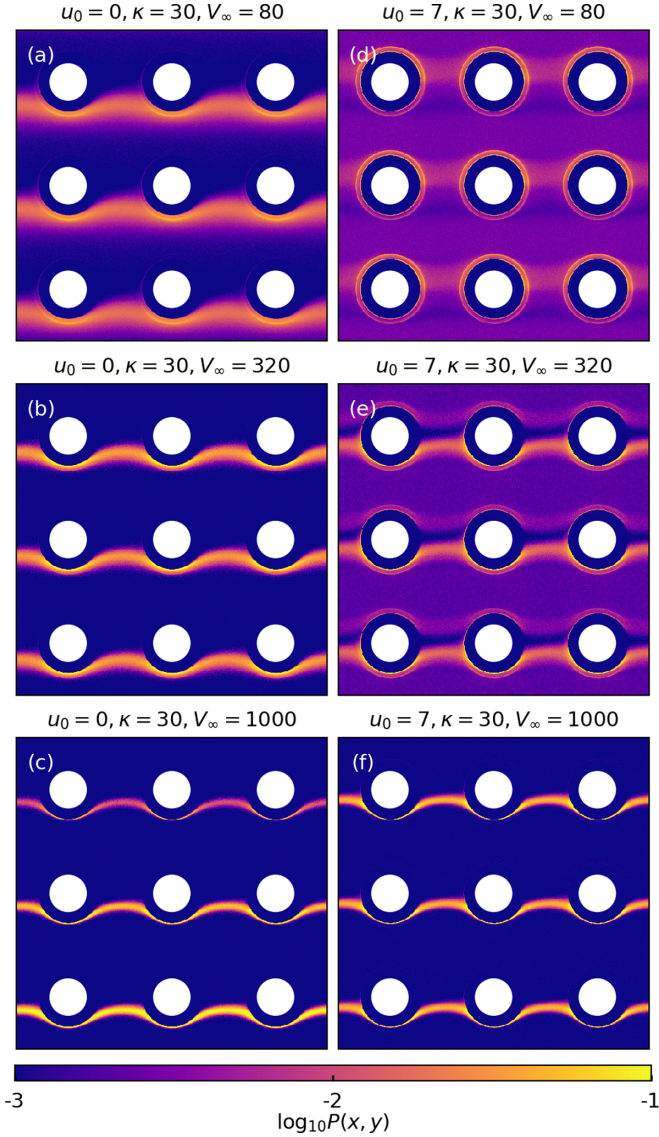FIG. 9. Log-probability density distributions of particle positions $\log_{10} P(x, y)$ for (a)–(c) $u_0 = 0$ and (d)–(f) $u_0 = 7$ at V_∞ of (a), (b) 80, (c), (d) 320, and (e), (f) 1000 for flow orientation $\theta = 1.25°$. The intense blue color corresponds to regions where $\log_{10} P(x, y) < -3$.

FIG. 10. Normalized longitudinal dispersion coefficient D_L/D_0 as a function of flow orientation θ in a square array with $\phi = 0.058$ for attractive potentials with $\kappa = 30$ and (a) $u_0 = 0$ and (b) $u_0 = 6$.

frustrates directional locking behavior at small $V_\infty \leqslant 320$ and shifts its onset to larger V_∞ [Figs. 9(d)–9(f)]. For small $V_\infty = 80$, particles advecting to the nanoposts are driven to the upper hemisphere of an adjacent post downstream by the attractions, thus frustrating directional locking [Fig. 9(d)]. Upon increasing V_∞, however, some of the particles are driven to the bottom hemisphere of the subsequent post by the stronger effect of advection in this region leading to partial directional locking [Fig. 9(e)]. At large $V_\infty = 1000$, advection becomes dominant and leads to nearly perfect directional locking [Fig. 9(f)]. Our results are qualitatively consistent with a recent study, which showed that the critical particle size for separation in DLD devices can be manipulated by controlling electrostatic interactions between particle and obstacles [55].
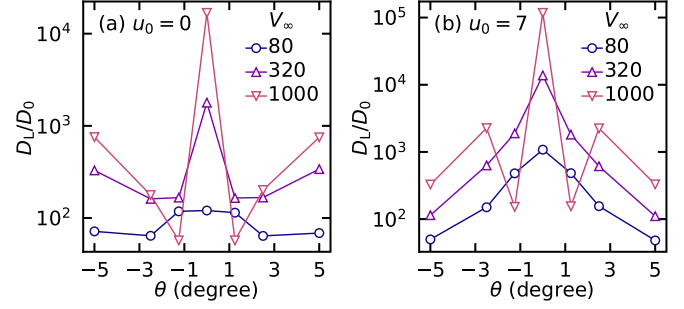
The frustration of directional locking at small V_∞ for $u_0 = 7$ arises from the competition between attractive and advective forces. At small $V_\infty = 80$, particles advecting to the nanoposts by the flow streamlines cannot leave from the bottom hemisphere of the post due to the strong attractive interactions. Particles are driven to the wake of the nanopost by the attractions and then transported along the flow streamlines to the upper hemisphere of the next nanopost. This process frustrates directional locking. Upon increasing V_∞, however, the probability of particles leaving from the bottom hemisphere of the nanopost increases due to the stronger effect of advection, leading to partial directional locking. For large $V_\infty = 1000$, advection becomes dominant and all particles leave from the bottom hemisphere of the nanopost, resulting in nearly perfect directional locking.

The changes in directional locking behavior arising from attractive interactions strongly affect longitudinal dispersion. In the absence of attractive interactions (i.e., $u_0 = 0$), D_L/D_0 exhibits nonmonotonic behavior due to directional locking [41] for all V_∞ as θ is perturbed away from $0°$, which corresponds to flow along the primitive lattice vector $\mathbf{a}$ [Fig. 10(a)]. For $u_0 = 7$, however, D_L/D_0 gradually decreases for $V_\infty \leqslant 320$ as θ is perturbed away from $0°$ [Fig. 10(b)]. The gradual decrease in D_L/D_0 reflects sampling of all flow streamlines by the particles and thus the frustration of directional locking by attractive interactions. By contrast, for $V_\infty = 1000$, advection dominates particle transport and D_L/D_0 exhibits nonmonotonic behavior as a function of θ due to directional locking [41]. Thus, attractive interactions frustrate directional locking at moderate flow rates ($V_\infty < 320$), and alter the trends of longitudinal dispersion as a function of flow orientations.

IV. CONCLUSION

We performed Stokesian dynamics simulations to investigate the effects of attractive interactions on the long-time transport properties of finite-sized particles within square arrays of nanoposts. Under quiescent conditions, the normalized diffusivity D_q/D_0 was negligibly affected by attractive interactions with the nanoposts for potential strength $u_0 \leqslant 3$. Upon further increasing u_0, D_q/D_0 exhibited a gradual downturn, followed by a sharp decrease for $u_0 \geqslant 5$. For $u_0 = 6$, D_q/D_0 steadily decreased with increasing potential range κ^{-1}. Under flow conditions, the characteristic residence time τ_R of particles near the nanoposts increased exponentially with

increasing attraction strength u_0 and decreases as the suspension velocity V_∞ increases. Consequently, for small to moderate Pe (Pe $<10^3$), increasing the potential strength u_0 led to a marked increase in the normalized longitudinal dispersion D_L/D_0 by up to two orders of magnitude. At large Pe (Pe $>10^3$), however, D_L/D_0 only increased weakly with u_0 due to the dominance of advection in this regime. By contrast, increasing the potential range k^{-1} while fixing u_0 resulted in a slight increase in D_L/D_0 at low Pe (Pe $<10^2$), but did not significantly affect dispersion at moderate to high Pe ($10^2 < $ Pe $< 10^4$). Finally, we examined the effects of attractions on directional locking. Attractive interactions frustrated directional locking behavior at small $V_\infty \leqslant 320$ and shifted the onset of this behavior to larger V_∞.

Our simulations provide insights into the effects of attractive interactions on the transport of finite-sized particles in ordered arrays, relevant to separation methods such as deterministic lateral displacement [56,57] and hydrodynamic chromatography [58–60]. The simple model reported in this study intentionally neglects features such as variability in nanopost size and spacing in the porous medium and physicochemical interactions between the particles, which may become relevant in specific systems (e.g., in disordered media or in concentrated suspensions). We anticipate that the computational approach employed in this study can be adapted to address the role of these factors in future work.

[1] M. Vallet-Regí, M. Colilla, I. Izquierdo-Barba, and M. Manzano, Molecules **23**, 47 (2017).

[2] F.-Y. Kong, J.-W. Zhang, R.-F. Li, Z.-X. Wang, W.-J. Wang, and W. Wang, Molecules **22**, 1445 (2017).

[3] H. ShamsiJazeyi, C. A. Miller, M. S. Wong, J. M. Tour, and R. Verduzco, J. Appl. Polym. Sci. **131**, 40576 (2014).

[4] M. Zarei, M. Zarei, and M. Ghasemabadi, TrAC Trends Analytic. Chem. **86**, 56 (2017).

[5] B. W. J. Pirok, N. Abdulhussain, T. Aalbers, B. Wouters, R. A. H. Peters, and P. J. Schoenmakers, Anal. Chem. **89**, 9167 (2017).

[6] R. Chen, R. Poling-Skutvik, A. Nikoubashman, M. P. Howard, J. C. Conrad, and J. C. Palmer, Macromolecules **51**, 1865 (2018).

[7] R. Chen, R. Poling-Skutvik, M. P. Howard, A. Nikoubashman, S. A. Egorov, J. C. Conrad, and J. C. Palmer, Soft Matter **15**, 1260 (2019).

[8] R. C. Roberts, R. Poling-Skutvik, J. C. Palmer, and J. C. Conrad, J. Phys. Chem. Lett. **9**, 3008 (2018).

[9] R. Poling-Skutvik, R. C. Roberts, A. H. Slim, S. Narayanan, R. Krishnamoorti, J. C. Palmer, and J. C. Conrad, J. Phys. Chem. Lett. **10**, 1784 (2019).

[10] R. C. Roberts, R. Poling-Skutvik, J. C. Conrad, and J. C. Palmer, J. Chem. Phys. **151**, 194501 (2019).

[11] D. L. Koch, R. G. Cox, H. Brenner, and J. F. Brady, J. Fluid Mech. **200**, 173 (1989).

[12] J. P. Gleeson, J. M. Sancho, A. M. Lacasta, and K. Lindenberg, Phys. Rev. E **73**, 041102 (2006).

[13] J. Herrmann, M. Karweit, and G. Drazer, Phys. Rev. E **79**, 061404 (2009).

[14] R. J. Phillips, W. M. Deen, and J. F. Brady, AIChE J. **35**, 1761 (1989).

[15] R. J. Phillips, W. M. Deen, and J. F. Brady, J. Colloid Interface Sci. **139**, 363 (1990).

[16] C. Reichhardt and C. J. Olson Reichhardt, Phys. Rev. E **69**, 041405 (2004).

[17] C. Reichhardt, C. J. Olson Reichhardt, and M. B. Hastings, Phys. Rev. E **69**, 056115 (2004).

[18] K. Lindenberg, A. M. Lacasta, J. M. Sancho, and A. Romero, New J. Phys. **7**, 29 (2005).

[19] A. M. Lacasta, J. M. Sancho, A. Romero, and K. Lindenberg, Phys. Rev. Lett. **94**, 160601 (2005).

[20] A. Lacasta, M. Khoury, J. M. Sancho, and K. Lindenberg, Mod. Phys. Lett. B **20**, 1427 (2006).

[21] K. Lindenberg, J. M. Sancho, A. M. Lacasta, and I. M. Sokolov, Phys. Rev. Lett. **98**, 020602 (2007).

[22] J. Frechette and G. Drazer, J. Fluid Mech. **627**, 379 (2009).

[23] C. Reichhardt and C. J. Olson Reichhardt, Phys. Rev. Lett. **106**, 060603 (2011).

[24] D. Hlushkou, F. Gritti, A. Daneyko, G. Guiochon, and U. Tallarek, J. Phys. Chem. C **117**, 22974 (2013).

[25] D. Hlushkou, F. Gritti, G. Guiochon, A. Seidel-Morgenstern, and U. Tallarek, Anal. Chem. **86**, 4463 (2014).

[26] J. Hansing and R. R. Netz, Macromolecules **51**, 7608 (2018).

[27] D. L. Koch and J. F. Brady, J. Fluid Mech. **154**, 399 (1985).

[28] J. Salles, J. F. Thovert, R. Delannay, L. Prevors, J. L. Auriault, and P. M. Adler, Phys. Fluids **5**, 2348 (1993).

[29] R. S. Maier, D. M. Kroll, R. S. Bernard, S. E. Howington, J. F. Peters, and H. T. Davis, Phys. Fluids **12**, 2065 (2000).

[30] D. Edwards, M. Shapiro, H. Brenner, and M. Shapira, Transp. Porous Media **6**, 337 (1991).

[31] H. P. A. Souto and C. Moyne, Phys. Fluids **9**, 2253 (1997).

[32] T. Stylianopoulos, B. Diop-Frimpong, L. L. Munn, and R. K. Jain, Biophys. J. **99**, 3119 (2010).

[33] D. Mangal, J. C. Conrad, and J. C. Palmer, AIChE J. **67**, e17147 (2021).

[34] T. Stylianopoulos, M.-Z. Poh, N. Insin, M. G. Bawendi, D. Fukumura, L. L. Munn, and R. K. Jain, Biophys. J. **99**, 1342 (2010).

[35] P. Bacchin, A. Marty, P. Duru, M. Meireles, and P. Aimar, Adv. Colloid Interface Sci. **164**, 2 (2011).

[36] T. Zhang, M. J. Murphy, H. Yu, H. G. Bagaria, K. Y. Yoon, B. M. Neilson, C. W. Bielawski, K. P. Johnston, C. Huh, and S. L. Bryant, SPE J. **20**, 667 (2015).

[37] C. V. Chrysikopoulos, P. K. Kitanidis, and P. V. Roberts, Transp. Porous Media **7**, 163 (1992).

[38] X. Yan, Q. Wang, and H. H. Bau, J. Chromatogr. A **1217**, 1332 (2010).

[39] L. Li, X. Yan, J. Yang, and Q. Wang, Appl. Energy **185**, 2168 (2017).

[40] S. C. James, L. Wang, and C. V. Chrysikopoulos, J. Hydrol. **566**, 735 (2018).

[41] D. Mangal, J. C. Palmer, and J. C. Conrad, Phys. Rev. E **104**, 015102 (2021).

[42] J. F. Brady and G. Bossis, Annu. Rev. Fluid Mech. **20**, 111 (1988).

[43] R. J. Phillips, J. F. Brady, and G. Bossis, Phys. Fluids **31**, 3473 (1988).

[44] M. Wang and J. F. Brady, J. Chem. Phys. **142**, 094901 (2015).

[45] N. Tufenkji and M. Elimelech, Langmuir **20**, 10818 (2004).

[46] F. Babayekhorasani, D. E. Dunstan, R. Krishnamoorti, and J. C. Conrad, Soft Matter **12**, 8407 (2016).

[47] M. P. Howard, A. Gautam, A. Z. Panagiotopoulos, and A. Nikoubashman, Phys. Rev. Fluids **1**, 044203 (2016).

[48] J. Hansing, C. Ciemer, W. K. Kim, X. Zhang, J. E. DeRouchey, and R. R. Netz, Eur. Phys. J. E **39**, 53 (2016).

[49] R. J. Phillips, Biophys. J. **79**, 3350 (2000).

[50] W. Chien and Y.-L. Chen, Soft Matter **12**, 7969 (2016).

[51] J. Frenkel, *Kinetic Theory of Liquids* (Dover, Mineola, NY, 1955).

[52] A. Felinger, J. Chromatogr., A **1184**, 20 (2008).

[53] P. Linse and N. Kallrot, Macromolecules **43**, 2054 (2010).

[54] J. Koplik and G. Drazer, Phys. Fluids **22**, 052005 (2010).

[55] K. K. Zeming, N. V. Thakor, Y. Zhang, and C.-H. Chen, Lab Chip **16**, 75 (2016).

[56] L. R. Huang, E. C. Cox, R. H. Austin, and J. C. Sturm, Science **304**, 987 (2004).

[57] J. McGrath, M. Jimenez, and H. Bridle, Lab Chip **14**, 4139 (2014).

[58] J. O. de Beeck, W. D. Malsche, P. D. Moor, and G. Desmet, J. Separat. Sci. **35**, 1877 (2012).

[59] A. Daneyko, D. Hlushkou, S. Khirevich, and U. Tallarek, J. Chromatogr. A **1257**, 98 (2012).

[60] A. M. Striegel and A. K. Brewer, Annu. Rev. Anal. Chem. **5**, 15 (2012).